USE OF BLACKBODY OPTICAL FIBER THERMOMETERS IN HIGH TEMPERATURE ENVIRONMENTS

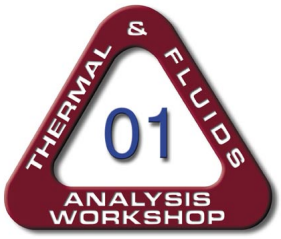

Matthew R. Jones and David G. Barker
Department of Mechanical Engineering
Brigham Young University

ABSTRACT

A blackbody optical fiber thermometer consists of an optical fiber whose sensing tip is given a metallic coating. The sensing tip of the fiber forms an isothermal cavity, and the emission from this cavity is approximately equal to the emission from a blackbody. Temperature readings are obtained by measuring the spectral intensity at the end of the fiber at two wavelengths. The ratio of these measurements is used to infer the temperature at the sensing tip. However, readings from blackbody optical fiber thermometers are corrupted by self-emission when extended portions of the probe are exposed to elevated temperatures. This paper describes two possible methods for correcting the problem due to self-emission by the fiber. The first method is two-fiber optical fiber thermometry. In this method, a second fiber is positioned parallel to the original fiber. The fibers are identical except that the second fiber has a reflecting coating instead of a blackbody cavity at its tip. Since both the emitting and reflecting fibers are exposed to the same thermal environment, measurements of the intensity at the end of the reflecting fiber can be used to eliminate error due to emission by the fiber. The second approach is spectral remote sensing. In this method, the intensity exiting the fiber is measured in portions of the visible and infrared spectrum. The measured spectral intensities are used to reconstruct the temperature profile along the fiber. Application of these techniques to the thermal control system of a microgravity furnace is discussed.

INTRODUCTION

Optical fiber thermometers (OFT) are devices that use photonic signals to sense temperatures. Compared to other temperature sensors, OFT have the following advantages:

- Long-term stability
- Immunity to electromagnetic interference
- High precision
- Capable of withstanding harsh environments

Several types of OFT have been developed (Kreider 1985). Interferometric sensors use the thermal expansion of an optical fiber to perturb a laser signal, and the temperature is inferred using interferometry. Fluoropitc sensors have a photoluminescent material attached to the active end of an optical fiber. An excitation pulse from a pulsed laser or flash lamp activates the sensing

tip, and the temperature is inferred from the decay time of the photoluminescent signal. Blackbody sensors consist of a high-temperature optical fiber with an opaque cavity attached to the sensing tip. The spectral radiative flux detected at the end of the fiber is related to the temperature of the cavity via Planck's law (Dils 1983). Fluoroptic and interferometric sensors are very precise, but their temperature ranges are limited by material properties. Blackbody sensors can operate over a wide range of temperatures, so blackbody sensors are generally used in high temperature applications.

An example of an application in which the use of blackbody OFT is highly desirable is in the thermal control system of microgravity furnaces that will fly on the International Space Station. The design of these furnaces is similar to that of a Bridgman furnace and consists of a heater core, insulation jacket, instrumentation, coolant loop components, a cold zone for directional solidification, and a quench zone for rapid quenching. A sketch of a preliminary design for a typical furnace's hot zone is shown in Fig. 1. The heater core contains four heated zones: Booster 1, Booster 2, Main and Guard. The sensor plate is cooled in order to maintain sensors and other instrumentation at acceptable operating temperatures. The cold zone is a water-cooled chill block (not shown) that is located adjacent to Booster 1. This design produces the high thermal gradients required for directional solidification experiments.

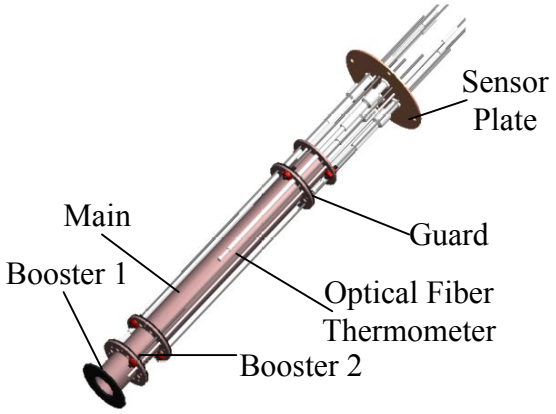

Figure 1. Hot zone assembly for a microgravity furnace

As shown in Fig. 1, the OFT are aligned with the axis of the furnace in these preliminary designs, and an extended portion of the fiber is exposed to elevated temperatures. Jones et al. (1999) showed that emission from portions of the fiber other than the sensing tip corrupt the temperature measurements under these conditions.

This paper describes two possible methods for correcting the problem due to self-emission by the fiber. The first method is two-fiber optical fiber thermometry (Jones et al. 2000). In this method, a second fiber is positioned parallel to the original fiber. The fibers are identical except that the second fiber has a reflecting coating instead of a blackbody cavity at its tip. Since both the emitting and reflecting fibers are exposed to the same thermal environment, measurements of the intensity at the end of the reflecting fiber can be used to eliminate error due to emission by the fiber. The second approach is motivated by previous studies in which spectral remote sensing

was used to determine the temperature profiles in semitransparent solids and high temperature gases (Chupp and Viskanta 1974, Hommert et al. 1975, Viskanta et al. 1975, Hommert and Viskanta 1978). In this method, the intensity exiting the fiber is measured in portions of the visible and infrared spectrum. The measured spectral intensities are used to reconstruct the temperature profile along the fiber.

BLACKBODY OPTICAL FIBER THERMOMETRY

A typical blackbody OFT is illustrated in Fig. 2 (Dils 1983). The probe consists of a sapphire (Al_2O_3) fiber whose sensing tip is given a metallic coating. The sensing tip of the fiber forms an isothermal cavity, so emission from this cavity is approximately equal to the emission from a blackbody. The other end of the fiber is attached to the detection system.

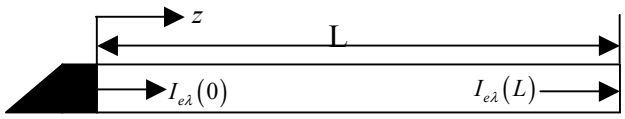

Figure 2. Schematic diagram for a blackbody optical fiber thermometer. The sensing tip $(z=0)$ is coated with a thin metallic film to create a small isothermal cavity at a temperature of T_0. The radiative flux emitted by the cavity, $I_\lambda(0)$, is approximately equal to the spectral emissive power of a blackbody, $I_{b\lambda}(T_0)$

An equation relating the spectral intensity at the end of the fiber to the spectral intensity emitted from the cavity is needed to infer the temperature at the sensing tip. The required relationship is obtained by modeling the fiber as an absorbing, emitting and non-scattering medium. The spectral intensity at each point along the fiber is given by the solution of Eq. 1 with the boundary condition specified by Eq. 2 (Brewster 1992).

$$\frac{dI_{e\lambda}}{dz} = -K_{a\lambda} I_{e\lambda} + K_{a\lambda} I_{b\lambda}\left(T(z)\right) \tag{1}$$

$$I_{e\lambda}(0) = I_{b\lambda}(T_0) \tag{2}$$

Solving for $I_{b\lambda}(T_0)$ gives

$$I_{b\lambda}(T_o) = I_{e\lambda}(t_{\lambda L})\exp\{t_{\lambda L}\} - \int_0^{t_{\lambda L}} I_{b\lambda}\left(T(t_\lambda)\right)\exp\{t_\lambda\}\,dt_\lambda \tag{3}$$

where $t_\lambda = K_{a\lambda} z$ and $t_{\lambda L} = K_{a\lambda} L$. The exponential in the first term on the right hand side of Eq. 3 corrects for the attenuation due to absorption of the intensity as it propagates along the fiber. The

integral on the right hand side of Eq. 3 represents noise due to emission by the fiber. The usual procedure is to assume that this integral is negligible.

$$I_{b\lambda}\left(T_o\right) \approx I_{b\lambda}\left(T_{bf}\right) = I_{e\lambda}\left(t_{\lambda L}\right)\exp\left\{t_{\lambda L}\right\} \tag{4}$$

Note that the estimate of the spectral blackbody intensity given by Eq. 4 is greater than the true value, so the measured temperature, T_{bf}, will be greater than the actual temperature, T_o.

The spectral radiative flux leaving the fiber is measured by the detector. The relationship between the measured value and the spectral intensity at the end of the fiber is

$$I_{e\lambda}\left(t_{\lambda L}\right) = \beta_\lambda M_{e\lambda} \tag{5}$$

where β_λ is a calibration factor and $M_{e\lambda}$ is the output from the detector. For the temperatures and the wavelengths of interest, Wien's limit may be used to approximate the spectral intensity of a blackbody,

$$I_{b\lambda}\left(T\right) \approx \frac{c_1}{\pi n^2 \lambda^5 \exp\left\{{}^{c_2}\!/_{n\lambda T}\right\}} \tag{6}$$

where c_1 and c_2 are the radiation constants and n is the refractive index of the fiber at the specified wavelength.

The temperature is obtained by making measurements at two wavelengths, λ_1 and λ_2. Using Eqs. 4 - 6, the ratio of $M_{e\lambda_1}$ to $M_{e\lambda_2}$ is

$$\frac{M_{e\lambda_1}}{M_{e\lambda_2}} = \frac{n_2^2 \lambda_2^5 \beta_{\lambda_2} \exp\left\{t_{\lambda_2 L}\right\} \exp\left\{\dfrac{c_2}{n_2 \lambda_2 T_{bf}}\right\}}{n_1^2 \lambda_1^5 \beta_{\lambda_1} \exp\left\{t_{\lambda_1 L}\right\} \exp\left\{\dfrac{c_2}{n_1 \lambda_1 T_{bf}}\right\}} \tag{7}$$

The measured temperature is obtained by solving Eq. 7 for the estimated temperature, T_{bf}.

$$T_{bf} = \frac{c_2\left(\dfrac{1}{n_2\lambda_2} - \dfrac{1}{n_1\lambda_1}\right)}{\ln\left[\left(\dfrac{n_1}{n_2}\right)^2 \left(\dfrac{\lambda_1}{\lambda_2}\right)^5 \dfrac{\beta_{\lambda 1} \exp\left\{t_{\lambda_1 L}\right\} M_{e\lambda_1}}{\beta_{\lambda 2} \exp\left\{t_{\lambda_2 L}\right\} M_{e\lambda_2}}\right]} \tag{8}$$

Recall that the integral in Eq. 3 represents the portion of the detected radiative flux that is due to emission by the fiber. This integral is negligible when the temperature of the fiber is low ($I_{b\lambda}\left(T\left(t_\lambda\right)\right) \approx 0$ for $t_\lambda \neq 0$) or the optical depth of the fiber is small $\left(t_{\lambda L} \approx 0\right)$. In situations similar to the furnace design illustrated in Fig. 1, the emission represented by the fiber is not negligible (Jones et al. 1999). This paper focuses on two possible methods of accounting for the effects due to emission by the fiber. The first approach is two-fiber optical fiber thermometry, and the second approach is spectral remote sensing.

TWO-FIBER OPTICAL FIBER THERMOMETRY

One possible method to accounting for the integral in Eq. 3 is to position a second fiber next to the original fiber as illustrated in Fig. 3. The fibers are identical except that the second fiber has a reflecting coating instead of a blackbody cavity at its tip. The first fiber is referred to as the emitting fiber, and the second fiber is referred to as the reflecting fiber.

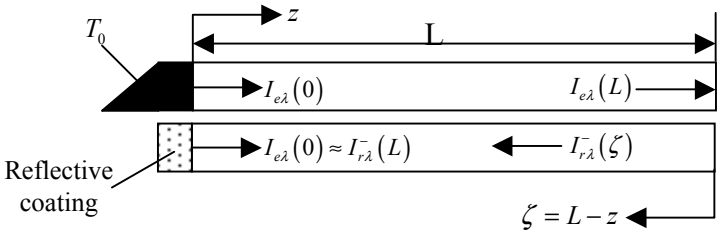

Figure 3. Schematic diagram for a two-fiber optical fiber thermometer

Since both the emitting and reflecting fibers are exposed to the same thermal environment, measurements of the spectral intensity at the end of the reflecting fiber can be used to eliminate error due to emission by the fiber. Three possible methods of using the data from the reflecting fiber to correct the temperature measurements have been developed (Jones et al. 2000). The most promising method is described below

The governing equation and boundary condition for the spectral intensity propagating along the reflecting fiber are given by Eqs. 9 and 10.

$$\frac{dI_{r\lambda}}{dz} = -K_{a\lambda} I_{r\lambda} + K_{a\lambda} I_{b\lambda}\left(T\left(z\right)\right) \tag{9}$$

$$I_{r\lambda}\left(0\right) = \rho_\lambda I_{r\lambda}^{-}\left(L\right) + \left(1-\rho_\lambda\right) I_{b\lambda}\left(T\left(0\right)\right) \tag{10}$$

Reflecting fibers can be fabricated by masking all but the tip of the fiber and sputtering a layer of MgO onto the fiber. The normal spectral reflectance of MgO is approximately 0.97 in the 0.4 μm to 1 μm spectral region (Touloukian and DeWitt 1972). Therefore, assuming $\rho_\lambda \approx 1$ the solution of Eqs. 9 and 10 gives

$$I_{r\lambda}(0) = I_{r\lambda}(t_{\lambda L})\exp\{t_{\lambda L}\} - \int_0^{t_{\lambda L}} I_{b\lambda}\left(T(t_\lambda)\right)\exp\{t_\lambda\}\,dt_\lambda \tag{11}$$

Since $I_{r\lambda}(0) = \rho_\lambda I_{r\lambda}^-(L) \approx I_{r\lambda}^-(L)$, a second expression for $I_{r\lambda}(0)$ is obtained by solving for the spectral intensity propagating along the reflecting fiber in the direction of the reflecting tip. The appropriate equation and boundary condition are

$$\frac{dI_{r\lambda}^-}{d\zeta} = -K_{a\lambda}I_{r\lambda}^- + K_{a\lambda}I_{b\lambda}\left(T(\zeta)\right) \tag{12}$$

$$I_{r\lambda}^-(0) = 0 \tag{13}$$

The boundary condition given by Eq. 13 is appropriate, because the end of the fiber connected to the detection system is maintained at a low temperature. Therefore, emission at the wavelengths of interest is negligible. Solving Eqs. 12 and 13 gives

$$I_{r\lambda}(0) \approx I_{r\lambda}^-(t_{\lambda L}) = \int_0^{t_{\lambda L}} E_{b\lambda}\left(T(t_{\lambda L} - t_\lambda)\right)\exp\{-t_\lambda\}\,dt_\lambda \tag{14}$$

Combining Eqs. 11 and 14 gives

$$\int_0^{t_{\lambda L}} I_{b\lambda}\left(T(t_\lambda)\right)e^{t_\lambda}dt_\lambda = I_{r\lambda}(t_{\lambda L})e^{t_{\lambda L}} - \int_0^{t_{\lambda L}} I_{b\lambda}\left(T(t_{\lambda L} - t_\lambda)\right)e^{-t_\lambda}dt_\lambda \tag{15}$$

Substituting Eq. 15 into Eq. 3 gives

$$I_{b\lambda}(T_0) = I_{e\lambda}(t_{\lambda L})e^{t_{\lambda L}} - \left[I_{r\lambda}(t_{\lambda L})e^{t_{\lambda L}} - \int_0^{t_{\lambda L}} I_{b\lambda}\left(T(t_{\lambda L} - t_\lambda)\right)e^{-t_\lambda}dt_\lambda \right] \tag{16}$$

As in Eq. 3., the first term on the right hand side of Eq. 16 corrects for the attenuation of the spectral intensity as it propagates along the fiber. The terms in brackets on the right hand side of Eq. 16 represent noise due to emission by the fiber. The integral represents the spectral intensity emitted by the fiber toward the reflecting tip that is subsequently reflected and transmitted to the detection system.

Subtracting Eq. 3 from Eq. 16 gives

$$I_{r\lambda}(t_{\lambda L})\mathrm{e}^{t_{\lambda L}} = \int_0^{t_{\lambda L}} \left[I_{b\lambda}\left(T(t_\lambda)\right)e^{t_\lambda} + I_{b\lambda}\left(T(t_{\lambda L} - t_\lambda)\right)e^{-t_\lambda} \right]dt_\lambda \tag{17}$$

An average temperature is defined such that

$$I_{b\lambda}\left(T_a\right)=\frac{1}{e^{t_{\lambda L}}-e^{-t_{\lambda L}}}\int_0^{t_{\lambda L}}\left[I_{b\lambda}\left(T\left(t_\lambda\right)\right)e^{t_\lambda}+I_{b\lambda}\left(T\left(t_{\lambda L}-t_\lambda\right)\right)e^{-t_\lambda}\right]dt_\lambda \tag{18}$$

Next, the average temperature is used to approximate the integral in Eq. 3. That is,

$$I_{b\lambda}\left(T_o\right)\approx I_{b\lambda}\left(T_{2f}\right)=I_{e\lambda}\left(t_{\lambda L}\right)e^{t_{\lambda L}}-I_{b\lambda}\left(T_a\right)\int_0^{t_{\lambda L}}e^{t_\lambda}dt_\lambda=I_{e\lambda}\left(t_{\lambda L}\right)e^{t_{\lambda L}}-I_{b\lambda}\left(T_a\right)\left(e^{t_{\lambda L}}-1\right) \tag{19}$$

Combining Eqs. 17 - 19 gives

$$I_{b\lambda}\left(T_o\right)\approx I_{b\lambda}\left(T_{2f}\right)=I_{e\lambda}\left(t_{\lambda L}\right)e^{t_{\lambda L}}-\frac{e^{t_{\lambda L}}-1}{e^{t_{\lambda L}}-e^{-t_{\lambda L}}}I_{r\lambda}\left(t_{\lambda L}\right)e^{t_{\lambda L}} \tag{20}$$

Similar to Eq. 5, the relationship between the spectral intensity at the end of the reflecting fiber and the measured value is

$$I_{r\lambda}\left(t_{\lambda L}\right)=\beta_\lambda M_{r\lambda} \tag{21}$$

Again, an approximate temperature is obtained by making measurements at two wavelengths, λ_1 and λ_2. Combining Eqs. 5-6 and Eqs. 20-21 gives

$$T_{2f}=\frac{c_2\left(\frac{1}{n_2\lambda_2}-\frac{1}{n_1\lambda_1}\right)}{\ln\left[\left(\frac{n_1}{n_2}\right)^2\left(\frac{\lambda_1}{\lambda_2}\right)^5\frac{\beta_{\lambda_1}e^{t_{\lambda_1 L}}\left(M_{e\lambda_1}-\frac{e^{t_{\lambda_1 L}}-1}{e^{t_{\lambda_1 L}}-e^{-t_{\lambda_1 L}}}M_{r\lambda_1}\right)}{\beta_{\lambda_2}e^{t_{\lambda_2 L}}\left(M_{e\lambda_2}-\frac{e^{t_{\lambda_2 L}}-1}{e^{t_{\lambda_2 L}}-e^{-t_{\lambda_2 L}}}M_{r\lambda_2}\right)}\right]} \tag{22}$$

SPECTRAL REMOTE SENSING

In this method, the intensity exiting the fiber is measured in portions of the visible and infrared spectrum. The measured spectral intensities are used to reconstruct the temperature profile along the length of the fiber. Based on Eq. 3, the temperature profile is related to the measured values through an integral equation.

$$\beta_{\lambda_i}M_{e\lambda_i}=I_{e\lambda}\left(t_{\lambda L}\right)=\exp\left\{-t_{\lambda_i L}\right\}\left[I_{b\lambda_i}\left(T_o\right)+\int_0^{t_{\lambda_i L}}\exp\left\{t_{\lambda_i}\right\}I_{b\lambda_i}\left(T\left(t_{\lambda_i}\right)\right)dt_{\lambda_i}\right] \tag{23}$$

An estimate of the temperature profile is obtained by inverting Eq. 23. This equation is classified as a Fredholm integral equation of the first kind. This type of equation is frequently encountered in the solution of inverse problems involving radiative transfer (Howell et al. 2000), and it is known that the solution to an equation of this type is not unique (Jones 2001).

Because there is not a unique solution, conventional gradient-based search methods are likely to become trapped in local minima and are generally ineffective in finding optimal solutions in cases such as this. A directed random search method such as a genetic algorithm is capable of finding the global optimal solution in complex, multi-dimensional search spaces. Genetic algorithms are based on the principle of natural selection or survival of the fittest. The structure of a typical genetic algorithm is shown in Fig. 4. The following paragraphs briefly describe the aspects of the implementation unique to this study. Detailed discussions of the fundamentals of genetic algorithms and descriptions of the wide variety of optimization problems successfully treated using genetic algorithms are available in the literature (Goldberg 1989, Pham and Karaboga 2000).

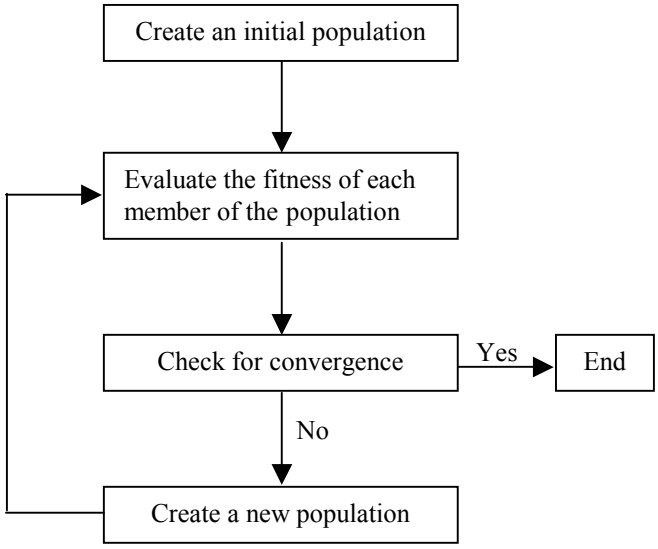

Figure 4. Flowchart for a simple genetic algorithm

SELECTION OF AN INITIAL POPULATION

An initial population of 100 possible temperature profiles was created by randomly perturbing an initial estimate of the temperature profile along the optical fiber.

THE FITNESS FUNCTION

The error for the j[th] possible temperature profile in the population is the rms value of difference between the measurements and the value of $\left(\beta_{\lambda_i} M_{\lambda_i}\right)_j$ obtained from Eq. 9 using the j[th] temperature profile.

$$\varepsilon_j = \frac{1}{N_\lambda} \sum_{i=1}^{N_\lambda} \sqrt{\left(\frac{\left(\beta_{\lambda_i} M_{\lambda_i}\right)_{measured} - \left(\beta_{\lambda_i} M_{\lambda_i}\right)_j}{\left(\beta_{\lambda_i} M_{\lambda_i}\right)_{measured}} \right)^2} \tag{24}$$

The smoothness of each temperature profile was quantified using the second finite differences.

$$s_j = \frac{2}{N_p - 2} \sum_{k=2}^{N_p - 1} \left| \frac{\left(T(z_{k+1}) - T(z_k)\right)\left(z_k - z_{k-1}\right) - \left(T(z_k) - T(z_{k-1})\right)\left(z_{k+1} - z_k\right)}{\left(z_{k+1} - z_{k-1}\right)\left(z_{k+1} - z_k\right)\left(z_k - z_{k-1}\right)} \right| \tag{25}$$

The fitness of the j[th] possible temperature profile was defined as

$$f_j = \frac{\varepsilon_{\max} - \varepsilon_j}{\varepsilon_{avg}} + \frac{s_{\max} - s_j}{s_{avg}} \tag{26}$$

where $\varepsilon_{\max}$ and ε_{avg} are the maximum and average values for the current generation and $s_{\max}$ and s_{avg} are the maximum and average values of the smoothness criterion for the current generation.

CREATION OF A NEW POPULATION

The possible temperature profile with the greatest fitness value and the possible temperature profile with the minimum error from the previous generation were copied directly into the new generation. If the most fit solution happened to be the solution with minimum error, two copies of the same solution would be placed in the new generation. This was necessary to avoid losing the solution with minimum error. The rest of the new generation was created using the two methods described below.

The first approach used the crossover and mutation operators to create the remaining possible temperature profiles (Goldberg 1989, Pham and Karaboga 2000). The crossover operation consists of selecting two possible temperature profiles according to their fitness values. A crossover site for each point in the temperature profile was randomly selected, and the portion of the temperature profile above the crossover site in the first possible profile was combined with the remaining portion of the second possible profile to create a new possible temperature profile. The mutation operator was applied after the new generation had been filled. The mutation operator consists of randomly selecting 1% of all the temperature values and then randomly perturbing it within a range of 800 K.

In the second approach, a smoothing operator was repeatedly applied to the possible temperature profile with the minimum error. Ten new possible profiles were created using the average of the temperature at a point with its two nearest neighbors. The next ten new possible profiles were created using the average of the temperature at a point with its four nearest neighbors. The remaining 78 new possible temperature profiles were created using the crossover and mutation operators as described above.

OPTICAL PROPERTIES OF SAPPHIRE

The spectral refractive index and absorption coefficient of Al_2O_3 must be known in order to evaluate the temperature at the sensing end of the OFT using Eq. 8 or Eq. 22 or to reconstruct the temperature profile along the OFT using Eq. 23. Maltison (1962) measured the refractive index of sapphire at 46 wavelengths between 0.2652 μm and 5.577 μm at room temperature. A three-term Sellmeier dispersion equation was developed based on these measurements, and this equation was used to calculate the refractive index as a function of wavelength. Brewster (1992) compiled a table of data regarding the imaginary part of the refractive index of sapphire from a variety of sources. The spectral absorption coefficients were calculated using Eq. 27 and linear interpolation of this data.

$$K_{a\lambda} = \frac{4\pi k}{\lambda} \tag{27}$$

Figure 5 shows the spectral refractive indices and absorption coefficients used in this study. Since the wavelength at which the peak emission occurs increases as the average temperature decreases, it is necessary to make measurements at longer wavelengths to reconstruct temperature profiles with lower average temperatures. Obtaining measurements at longer wavelengths is difficult due to increased absorption, so it is expected that the reconstruction of the temperature profile will be more difficult as the average temperature decreases.

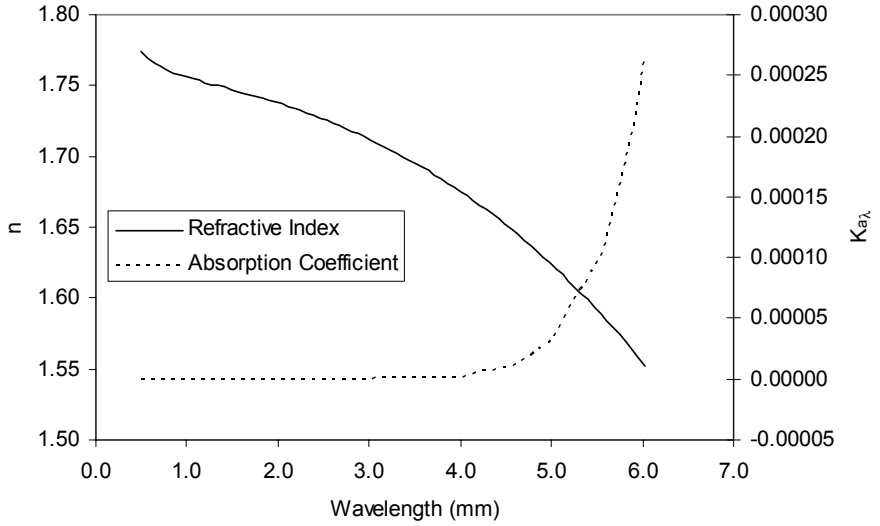

Figure 5. Refractive Index (n) and Absorption Coefficient ($K_{a\lambda}$) as a function of wavelength for Al_2O_3

Gryvnak and Burch (1965) reported significant increases in the absorption coefficient with temperature above 1200 C. However, data regarding the variation of the absorption coefficient with temperature below 1200 C is not available for the spectral range of interest, so it was assumed that the absorption coefficient was independent of temperature in this study.

SIMULATED TEMPERATURE MEASUREMENTS

Three typical axial temperature profiles for the microgravity furnace illustrated in Fig. 1 were obtained from a detailed thermal model (NASA-MSFC et al. 1999). Simulated measurements of the spectral radiative flux were calculated using these temperature profiles and Eq. 23 for a number of wavelengths. The spectral radiative flux is defined as the product of the spectral intensity and the solid angle defined by the numerical aperture of the optical fiber.

$$E_{e\lambda} = I_{e\lambda}\left(t_{\lambda L}\right)\Delta\Omega = \beta_{\lambda} M_{e\lambda}\Delta\Omega \tag{28}$$

For Cases 1 and 2, 50 different wavelengths between 0.5 μm and 4.0 μm were used. This spectral region includes all the wavelengths for which the emission was significant. For Case 3, 65 wavelengths between 0.5 μm and 5.0 μm were used to account for the peak wavelength shift. The wavelengths used in the two-fiber approach were 0.8 μm and 0.95 μm. The temperature measured using the standard approach to blackbody optical fiber thermometry is compared with the temperatures obtained using two-fiber optical fiber thermometry and remote sensing in Table 1.

Table 1. Simulated Temperature Measurements

Case	T_o (K)	T_{bf} (K)	T_{2f} (K)	T_{rs} (K)
1	1440	1458	1438	1441
2	1169	1200	1169	1169
3	877	895	877	878

The errors in the measured temperatures obtained using the standard approach to blackbody OFT vary between 1% to 3%. The larger errors occur when portions of the fiber are at temperatures greater than the temperature of the sensing tip (Cases 2 and 3). Note that, as predicted by comparing Eqs. 3 and 4, the measurements obtained using the standard approach are biased toward higher values.

The two-fiber approach eliminated the errors in Cases 2 and 3 and greatly reduced the error in Case1. The tip temperature was also accurately measured (to within 0.1%) using the remote sensing approach in each of the three cases.

The reconstructed temperature profiles obtained using the remote sensing approach are compared with the actual temperature profiles in Figs. 6 - 8. The initial estimates used to obtain these results are also shown in these figures. As expected, the reconstructed temperature profile is more accurate when the profile has a higher average temperature. In the worst case (Case 3), the maximum deviation of the reconstructed temperature profile from the actual temperature profile

was 5.3% in the high temperature region and 16.1% in the low temperature region. The average deviation between the actual temperature profile and the reconstructed temperature profile was 2.6% in this case.

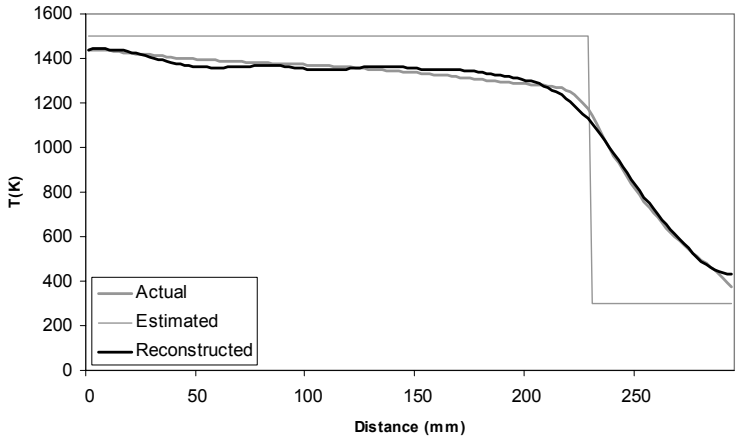

Figure 6. Reconstructed temperature profile for Case 1

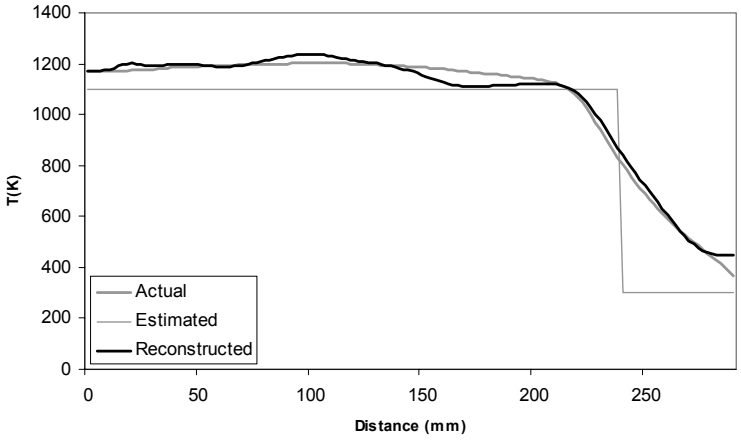

Figure 7. Reconstructed temperature profile for Case 2

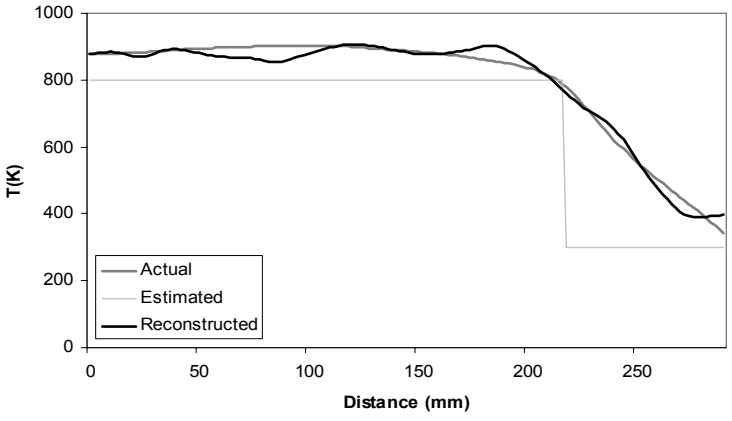

Figure 8. Reconstructed temperature profile for Case 3

Although the reconstructed temperature profiles differ from the actual temperature profile, the spectral radiative fluxes calculated using the actual temperature profile are in nearly perfect agreement with the spectral radiative fluxes calculated using the reconstructed temperature profile. Figure 9 compares the spectral radiative fluxes for the actual temperature profile and the reconstructed profile obtained for Case 3. The maximum deviation was 1.98% at 4.77 μm. The average deviation was 0.44%. The kink in Figure 9 is due to the rapid increase in the spectral absorption coefficient for wavelengths greater than 4.0 μm (see Figure 5).

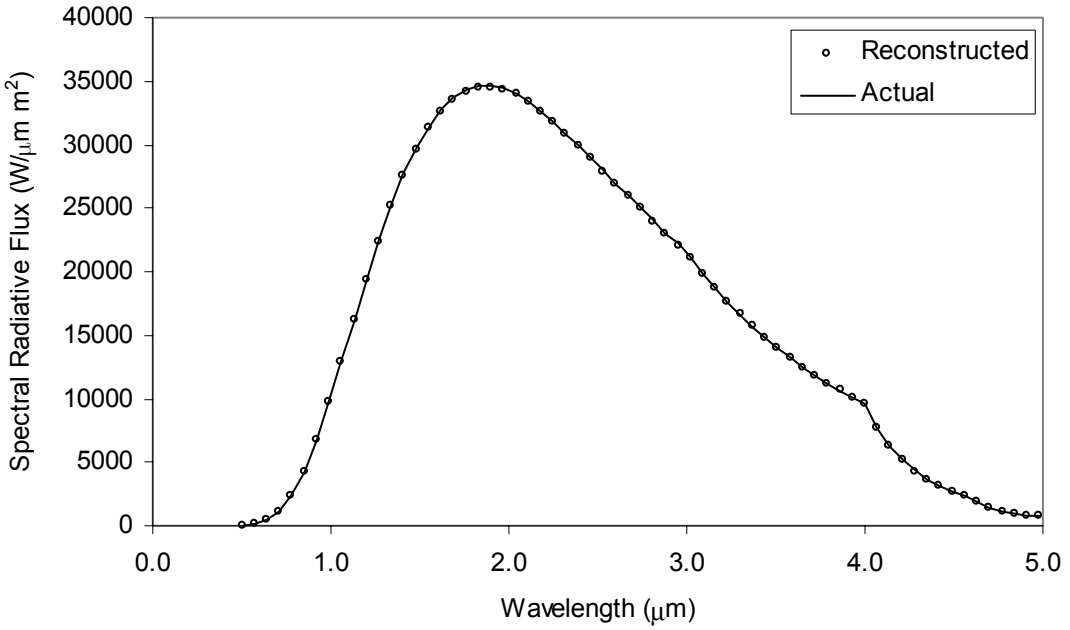

Figure 9. Spectral radiative flux for the reconstructed profile of Case 3

SUMMARY AND CONCLUSIONS

The use of blackbody optical fiber thermometers offers a number of advantages, but errors due to self-emission by the fiber prevent the use of the standard approach in applications where extended portions of the fiber are exposed to elevated temperatures. This paper described two methods that eliminate the errors due to emission by the fiber.

Two-fiber OFT uses a second fiber with a reflecting tip to estimate the spectral intensity emitted by the fiber. This approach eliminates the bias toward higher temperatures that occurs when the standard approach to blackbody OFT is employed.

The remote sensing method can be used to accurately determine the temperature at the tip of a blackbody OFT. The approach may also be used to estimate the temperature profile along the entire length of the fiber. For the cases considered in this paper, the reconstructed temperature profile was accurate to within approximately 5% in the high temperature region and to within approximately 16% in the low temperature region.

REFERENCES

Brewster, M. Q. 1992, *Thermal Radiative Transfer & Properties*, John Wiley & Sons, New York.

Dils, R. R. 1983, "High-temperature optical fiber thermometry," *Journal of Applied Physics*, Vol. 54 No. 3, pp. 1198 - 1201.

Chupp, R. E. and Viskanta, R. 1974, "Development and Evaluation of a Remote Sensing Technique for Determining the Temperature Distribution in Semitransparent Solids," *ASME Transactions – Journal of Heat Transfer,* Vol. 96, No. 3, pp. 391-397.

Gryvnak, D. A. and Burch, D. E. 1965, "Optical and Infrared Properties of Al_2O_3 at Elevated Temperatures," *Journal of the Optical Society of America*, Vol. 55 No. 6, pp. 625 - 629.

Goldberg, D. E., 1989, *Genetic Algorithms in Search, Optimization, and Machine Learning*, Addison-Wesley, Reading MA.

Hommert, P. J., Viskanta, R., and Chupp, R. E. 1975, "Application of Spectral Remote-Sensing Method for Recovering Temperature Distribution in Glass," *Journal of the American Ceramic Society*, Vol. 58, pp. 58-62.

Hommert, P. J. and Viskanta, R. 1978, "High Temperature Gas Diagnostics by Spectral Remote Sensing," International Journal of Heat and Mass Transfer, Vol. 21, pp. 769 – 781.

Howell, J. R., Ezekoye, O. A., and Morales, J. C. 2000, "Inverse Design Model for Radiative Heat Transfer," ASME Transactions – Journal of Heat Transfer, Vol. 122, No. 3, pp. 492 – 502.

Jones, M. R., Farmer, J. T., and Breeding, S. P. 1999, "Evaluation of the use of optical fiber thermometers for thermal control of the quench module insert," *Proceedings of the Thermal & Fluids Analysis Workshop*, Sep. 13 – 17, Huntsville, AL.

Jones, M. R., Farmer, J. T., and Breeding, S. P. 2000, "Two-Fiber Optical Fiber Thermometry," *Proceedings of IMECE: 2000 International Mechanical Engineering Congress and Exposition*, Nov. 5-10, Orlando, FL.

Jones, M. R. 2001, "Reconstruction of the Temperature Profile Along an Optical Fiber Thermometer," to appear in *Proceedings of IMECE: 2001 International Mechanical Engineering Congress and Exposition*, Nov. 11-16, New York, NY.

Kreider, K. G. 1985, "Fiber-Optic Thermometry," *Applications of Radiation Thermometry, ASTM STP 895*, J. C. Richmond and D. P. DeWitt, Eds. American Society of Testing and Materials, Philadelphia, pp. 151 -161.

Maltison, I. H. 1962, "Refraction and Dispersion of Synthetic Sapphire," *Journal of the Optical Society of America*, Vol. 52 No. 12, pp. 1377 – 1379.

NASA-MSFC, Tec-Masters Inc., Sverdrup Technologies 1999, *Thermal Design Data Book, Quench Module Insert, Preliminary Design Review*.

Pham, D. T. and Karaboga, D. 2000, *Intelligent Optimisation Techniques: Genetic Algorithms, Tabu Search, Simualted Annealing and Neural Networks*, Springer, London.

Touloukian, Y. S. and DeWitt, D. P. (eds.) 1972, *Thermal Radiative Properties: Nonmetallic Solids*, vol. 8 of *Thermophysical Properties of Matter*, Plenum Press, New York.

Viskanta, R., Hommert, P. J., and Groninger, G. L. 1975, "Spectral Remote Sensing of Temperature Distribution in Semitransparent Solids Heated by an External Radiation Source," Applied Optics, Vol. 14, No. 2, pp. 428 – 437.

CONTACT

Matthew R. Jones is an Assistant Professor in the Department of Mechanical Engineering at Brigham Young University. His email address is mrjones@et.byu.edu, and his phone number is 801-378-3070. David G. Barker is a senior majoring in mechanical engineering at Brigham Young University. His email address is dbarker@byu.edu, and his phone number is 801-378-3051.

NOMENCLATURE

c_1, c_2	Radiation constants
$E_{e\lambda}$	Spectral radiative flux
f	Fitness function
$I_{b\lambda}$	Spectral blackbody intensity
$I_{e\lambda}$	Spectral intensity in the emitting fiber
$I_{r\lambda}$	Spectral intensity in the reflecting fiber
i, j, k	Indices
$K_{a\lambda}$	Spectral absorption coefficient for the optical fiber
L	Length of the optical fiber
$M_{e\lambda}$	Measurement from the detector output
N_p	Number of points in the temperature profile
N_λ	Number of wavelengths
n	Real part of refractive index for Al_2O_3
k	Imaginary part of refractive index for Al_2O_3
s	Smoothness criterion
t_λ	Spectral optical length of the optical fiber
$t_{\lambda L}$	Total spectral optical depth of the optical fiber
$T(t_\lambda)$	Temperature profile
T_{bf}	Measured temperature obtained using the standard method
T_o	True temperature of the sensing tip
T_{rs}	Measured temperature obtained using the remote sensing method
T_{2f}	Measured temperature obtained using the two-fiber method

T_m Measured temperature of the sensing tip

z Distance along the axis of the fiber

β_λ Calibration factor

$\Delta\Omega$ Solid angle defined by the numerical aperture of the fiber

ε RMS difference between the measured and calculated radiative fluxes.

λ Wavelength

ρ_λ Spectral reflectivity of the reflective coating